Journal of Colloid and Interface Science 628 (2022) 205–214

Contents lists available at ScienceDirect

Journal of Colloid and Interface Science

journal homepage: www.elsevier.com/locate/jcis

Statistical thermodynamics in reversible clustering of gold nanoparticles. A first step towards nanocluster heat engines

Stefano A. Mezzasalma [a,b,*], Joscha Kruse [c], Amaia Iturrospe Ibarra [d], Arantxa Arbe [d], Marek Grzelczak [c,*]

[a] Materials Physics Division, Optics Laboratory, Ruđer Bošković Institute, Bijenička cesta 54, 10000 Zagreb, Croatia
[b] Lund Institute for advanced Neutron and X-ray Science (LINXS), Lund University, IDEON Building: Delta 5, Scheelevägen 19, 223 70 Lund, Sweden
[c] Centro de Física de Materiales (CSIC-UPV/EHU) and Donostia International Physics Center (DIPC), Manuel Lardizabal Ibilbidea 5, 20018 Donostia-San Sebastián, Spain
[d] Centro de Física de Materiales (CSIC-UPV/EHU), Manuel Lardizabal Ibilbidea 5, 20018 Donostia-San Sebastián, Spain

GRAPHICAL ABSTRACT

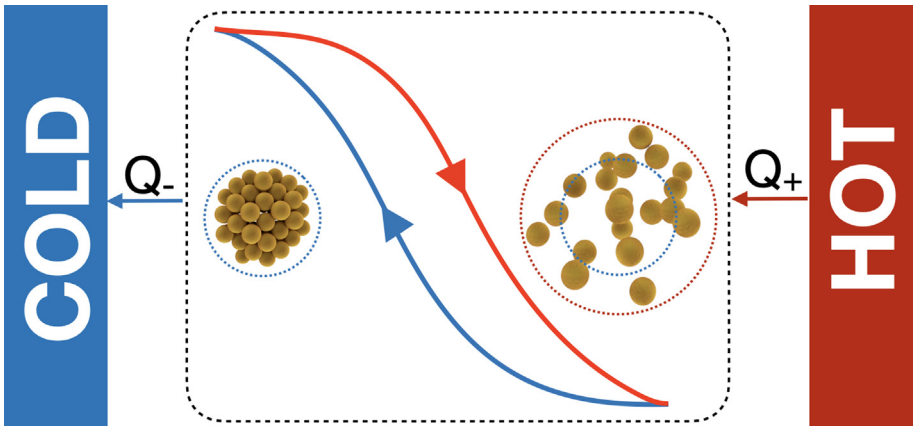

ARTICLE INFO

Article history:
Received 31 March 2022
Revised 8 June 2022
Accepted 6 July 2022
Available online 21 July 2022

Keywords:
Au nanocolloids
Reversible clustering
Transient equilibrium mapping
Hysteresis
Thermodynamic cycles
Statistical mechanics
Heat engines

ABSTRACT

A statistical thermodynamics variational criterion is propounded to study thermal hysteresis in reversible clustering of gold (Au) nanoparticles. Experimentally, a transient equilibrium mapping analysis is employed to characterize it thermodynamically, further measurements being performed at the nanostructural and electrochemical levels (UV-Vis-NIR spectra, SLS/SAXS, zeta potential). Theoretically, it is successfully interpreted as a thermodynamic cycle, prompting that nanoclusters has potential to produce useful work from heat and paving the way to nanoclustering heat engines. By taking into account the virial expansion of hysteretic pressure, an entropy measure is deduced for a dilute system with given virial coefficients. This allows us to figure out the role of relevant interparticle potential parameters (i.e. surface potential, nanoparticle size, Debye's length, Hamaker energy) in both isothermal and isochoric variations at the onset of hysteresis. Application to spherical Au nanoparticles in watery salt solution (NaCl) is developed when an ad-hoc (DLVO) pairwise potential governs the second virial coefficient at the nanoscale. In particular, the variational criterion predicts a pressure drop between heating and cooling paths which is likely at the base of some energy redistribution (e.g. ordering/restructuring of electric double

* Corresponding author.
E-mail addresses: stefano.mezzasalma@irb.hr (S.A. Mezzasalma), marek.g@csic.es (M. Grzelczak).

https://doi.org/10.1016/j.jcis.2022.07.037

layers). We found an integrating factor that is able to numerically predict the existence of a critical value for the initial salt concentration maximizing the hysteretic area, and the effect of nanoparticle size on the cycle extent.

1. Introduction

Hysteresis phenomena are ubiquitous in all of natural and engineering sciences – ranging from ferromagnetism [1] to ferroelectricity [2], from elastic [3] to plastic [4] and piezoelectric materials [5], from semiconductors [6] to superconductivity [7], from electron transport [8] to optical [9] processes – covering a phenomenology that spans from electron to geological scales. They are found in relevant applications in solid-state memory-storage devices and to support biological functions, as cell division, by means of noise resilience [10,11]. More specifically to colloid and interface science, hysteresis phenomena were and are intensively studied in subject matters of both traditional and nowadays interests, i.e. gas-solid adsorption [12,13], wetting and contact angle hysteresis with applications [14–17], capacitive current-voltage behaviors in bio-devices [18] and reversible aggregation of colloid particles [19], whose understanding is also noticeable for various molecular recognition processes in life sciences (e.g. cell adhesion and motility versus clustering of peptide motifs at the nanoscale) [20,21].

The unambiguous definition of a hysteretic phenomenon mostly rests on control theory and functional analysis (e.g. scalar or vector Preisach & Krasnoselskii approaches) [22], but it is the specific mechanism that often inspires or dictates the formalism to be worked out. This is definitely reasonable, as the response specificity to a given stimulus is essential for tailoring a smart nanosystem (e.g. as actuators, catalysts, sensors and biosensors). On the other hand, formulating a physical theory which is capable to interpret a wide class of hysteresis phenomena in the largest possible generality actually remains a non-trivial task. Enriching the matter then is the obvious classifications into irreversible and reversible mechanisms, into rate-dependent and rate-independent responses. In the first, where the hysteresis concept finds a more widespread definition, loop areas reflect the extent of dissipation events, while it is maybe more appropriate in the second to speak about multistability of states or thermodynamic cycles. Alongside, rate-dependent mechanisms are often source of nonlinearity, as in piezoelectric actuators [23], and were detected in pH-driven clustering of gold (Au) nanoparticles stabilized with carboxylated alkanethiols, poly-L-lysine and thermoresponsive polymers [24–26]. Rate-independent behaviors are more typical instead of homeostatic materials, memory storage, autonomous chemical reactions and DNA-coated nanoparticles undergoing melting/freezing transitions [27–29]. In most of these situations, however, an analysis of entropy and free energy functions is expected to be crucial for a deep inquiry, and specially in a nanoscopic system, where physical or chemical variables may mutually interact in large numbers to raise an extraordinarily rich phenomenological picture [30].

About one decade ago, a hysteresis loop in the variable pH was brought into light from experiments on liquid solutions of nanoparticles functionalized with ionizable ligands [31]. At a fixed pH, one may find nanoparticles in two different colloid states (say, dispersed and aggregated). Nanoparticles in a given state may conversely display two different pH values. The cycle was reported to be reversible and interpreted by an ingenious asymmetric trend for the radial interparticle force (F), crudely summing up as follows:

$$\begin{aligned} F(r) &< 0 \quad \forall r \quad \text{(aggregation)} \\ F(r) &> 0 \quad r \to 0^{+} \quad \text{(dispersion)} \end{aligned} \tag{1}$$

While no potential barrier establishes upon decreasing pH, dispersion of aggregated nanoparticles would be settled by a purely repulsive potential at the origin. As clustering depends on F, and the latter on pH, the asymmetry in Eq. (1) resulted into distinct ascending/descending curves.

Here, statistical thermodynamics is invoked in a hysteretic model of the thermal type for reversible clustering of Au nanoparticles. A variational condition will be inferred to readdress this matter with an ample generality, ultimately framing nanoclustering in the context of thermodynamic cycles (i.e. heat engines) and the consequent search of their maximum efficiency. Au nanoparticles are selected as a suitable experimental system, because of the chemical robustness they can bear upon harsh conditions, and their optical sensitivity to colloidal phase changes [32]. Finally, this research could be insightful to get a comparison between the nanocluster and single particle levels, where microscopic motors rely on random energy transfers and transient entropy decreases, requiring a reinterpretation of the usual thermodynamic bounds [33,34].

2. Hysteresis Experiments and Discussion

Gold nanoparticles (13.4 nm in diameter) stabilized with bis(p-sulfonato- phenyl)-phenylphosphine (BSPP) undergo reversible clustering when the solution is brought to low temperature (Fig. 1a) [35]. Although tracking the change of optical properties suffices to study the responsiveness of the system and thus its hys-

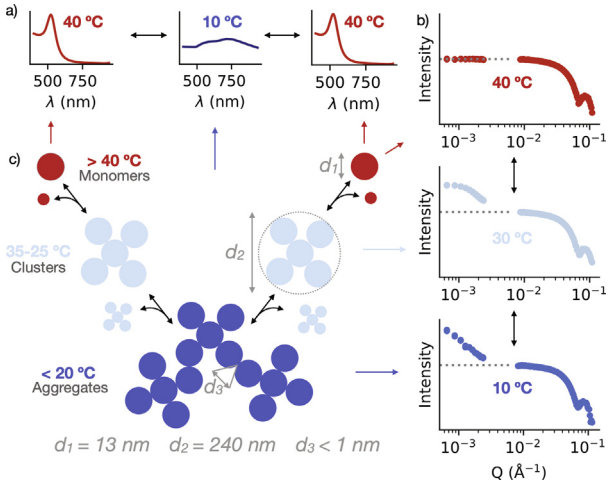

Fig. 1. Temperature-driven reversible aggregation of spherical Au nanoparticles. (a) UV-Vis-NIR spectra of dispersed (40 °C) and aggregated (10 °C) colloidal Au solution showing recovery of initial optical properties. (b) Temperature-dependent evolution of scattering intensity (combined SLS and SAXS results) versus the modulus of the scattering vector Q, showing colloidally dispersed (40 °C) clustered (20 °C) and aggregated (10 °C) nanoparticles. (c) Schematic description of aggregation process. Colloidally stable nanoparticles above 40 °C form cluster of ~ 240 nm below 35 °C. A further temperature drop below 25 °C causes aggregation. Temperature reversal brings the particles back to initial state.

teresis (*vide infra*), we measured static light scattering (SLS) to get an insight into the structure of aggregates at given temperature (Fig. 1b). Below 35 °C, nanoparticles formed stable clusters of 240 nm in diameter (Fig. 1b middle), resembling a scenario published recently in which the cluster growth was explained by the attachment of individual nanoparticles, monomers [36]. Further temperature drops below 20 °C led to the formation of open-structure aggregates that grew through the attachment of preformed clusters (Fig. 1b bottom). Small Angle X-ray Scattering (SAXS) analysis showed that the distance between the nanoparticles is below 1 nm. Heating of the sample reverses the process. To gain a more quantitative insight into the hysteretic response we performed the so-called transient equilibrium mapping [37], a spectroscopic method that comprises the rising and lowering of the sample temperature to allow the system to pass through the transient equilibrium on each up- and down- scan (Fig. 2a). By knowing the number of particles in the system (monomer concentration) and extracting the extrema of each cycle, we determined the value of ΔH and ΔS through Van't Hoff analysis (Fig. 2b). The analysis shows the aggregation of nanoparticles, under the present conditions, is a spontaneous process. The hysteretic response of the system depends on the salt concentration. The transient equilibrium mapping in Fig. 2a was accomplished at 100 mM of NaCl. The value of ζ-potential at this salt concentration received slightly negative values at low temperature range (Fig. 2b). On contrary, at lower salt concentration (e.g., 25 mM), there is a steep change of the ζ-potential toward negative values when temperature is decreased. No significant reversible aggregation at this concentration value was however observed (Supporting Information Fig. 2). Best fit analysis of these behaviors and other remarks are reported through Supporting Information F2-3. We may argue that during the decrease of temperature (no salt) free BSPP molecules can arrange on the nanoparticles surface leading to the increase of surface coverage and thus to a more negative ζ-potential. On contrary, the presence of salt screens the surface charge leading to more neutral potential over the entire temperature range, favoring clustering and aggregation.

The data hereby illustrated provide with further indications about this complex nanoclustering phenomenon, and will be employed to verify the forthcoming theoretical predictions. We will see how the transient equilibrium mapping analysis conforms to the thermodynamic interpretation of hysteresis. Evaluations of the average nanocluster size then will agree with SLS and SAXS results, while the quantitative behavior of ζ- potentials will be successfully exploited to model the areas of hysteresis loops. Other thermodynamic quantities could be obtained from appropriate combinations of entropy and enthalpy functions with thermodynamic variables or parameters.

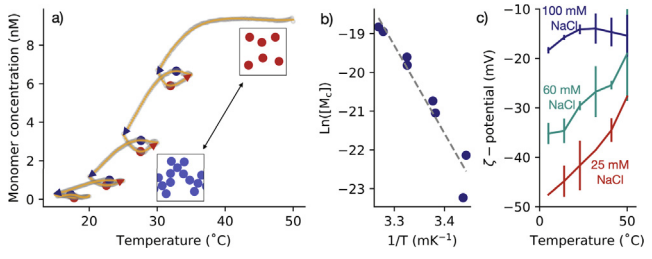

Fig. 2. Hysteretic aggregation of Au nanoparticles. (a) Transient equilibrium mapping with marked maxima (blue) and minima (red) of each cooling (blue arrows) and heating (red arrows) cycle. (b) Van't Hoff analysis of dispersion data in a) giving $\Delta H_0 = 188$ kJ/mol and $\Delta S_0 = 461$ J/(mol K). c) Change of ζ-potential versus temperature for salt concentrations with values 25, 60 and 100 mM. From a quantitative point of view, behaviors in (a) do not identify any of the typical textbook thermodynamic cycles. Wishing to make a qualitative choice, an inspection in the (T,S) plane shows the least different cyclic transformation here seems to be Rankine's.

3. Hysteresis Theory

3.1. Thermodynamic Hysteresis Condition

A first point to be discussed, where absolute temperature (T) takes the role of the experimentally independent variable, is hysteresis versus spontaneity. To fix the ideas, consider a mean number of (N) nanoparticles joint into a representative nanocluster, which organizes into a given ensemble of dispersion/aggregation states at different temperature and volume coordinates (V,T). The entropy function (S) of clustering will augment with temperature as, to a good approximation, the partition function may be factored into translational, rotational and vibrational parts, each increasing with increasing T, i.e. with higher dispersion degree [38]. With regard to enthalpy (H), for stabilized nanoparticles to aggregate upon salt addition to a liquid solution, the total process should be endothermic ($\Delta H_t > 0$) and comprise three main heat contributions, $\Delta H_t = \Delta H + \Delta H_d + \Delta H_\pm$. Either nanoparticle or salt dilutions are also endothermic ($\Delta H_d,\ \Delta H_\pm > 0$), the latter providing with the dominant term, thence aggregation should be exothermic ($\Delta H < 0$) [39]. This was also confirmed by the transient equilibrium mapping analysis presented in the experimental section, returning positive dispersion enthalpy and entropy, i.e. $\Delta H_0 = 75.4\ k_B T_r, \Delta S_0 = 55.4\ k_B$ ($T_r \approx 300$ K).

We now posit the thermal behavior of the absorbance to reflect a transformation in the (T,S) plane, and check the consistency of this assumption via the conditions on the Gibbs free energy ($G = H - TS$) for the spontaneity of a thermodynamic process. A useful diagram to refer to can be found in Fig. (3).

The aim is to verify if the loop, called hysteresis, met in reversible [35,31] nanoparticle assembly/disassembly may approach or be framed as a thermodynamic cycle, S being a state function e.g. of (T,V). The clockwise direction in which the cycle progresses (Fig. 3) then is guaranteed by the fact that, at equal values of T, the aggregation state (or assembly degree [35]) of nanoclusters is greater along heating curves, thus with lower S. Obviously, this can be an idealized picture, which can be useful however to argue whether nanoclustering has the potential to act as a heat engine and produce some useful work. We will see, after inquiring all

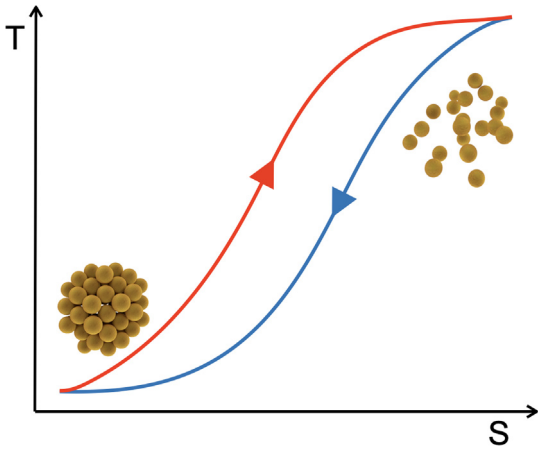

Fig. 3. Thermodynamic prototype of nanoclustering phenomena in (T,S) plane. Note the clockwise direction of the cycle, due to higher aggregation states (at equal T) along the heating curve (in red), assigning the system a character of heat engine. According to previously adopted experimental conventions, the initial state (i) is taken at higher temperatures and brought to lower values (f) upon cooling (in blue).

the model predictions against experiments, that the answer is positive.

Based on the previous arguments on S and H, in a descending (or aggregation) cooling path ($i \to f$) one should jointly have $\Delta S < 0$ and $\Delta H < 0$, both provisions needing to be reverted in the opposite direction of an ascending (or dispersion) heating path ($f \to i$), i.e. $\Delta S > 0$ and $\Delta H > 0$. In either case the principle $\Delta G < 0$ is non-trivially fulfilled, leading to:

$$\begin{array}{rcll} T & < & |\Delta H/\Delta S| & \text{(aggregation)} \\ T & > & |\Delta H/\Delta S| & \text{(dispersion)} \end{array} \tag{2}$$

and taking the place of former Eqs. (1). Such inequalities can prove that the area of a back and forth cycle is not zero, connecting the amount of work energy exchanged by the nanoparticle system with the environment:

$$\oint TdS = -\int_i^f T|dS| + \int_f^i T|dS| > -\int_i^f |dH| + \int_f^i |dH| \tag{3}$$

or:

$$\oint TdS \geqslant \oint dH \tag{4}$$

where the equality sign holds with no hysteresis. For a reversible process, as it was supposed for clustering of nanocolloids with specific interparticle linkages [31,19] (via e.g. surface ligands or polymer brushes) one has $dH = TdS + Vdp$ and the former relation rewrites:

$$\oint Vdp \leqslant 0 \tag{5}$$

p being pressure. Interestingly, absence of hysteresis here corresponds to an unperturbed (or stationary) condition resembling Maxwell's equal area rule in (p, V) representation, typically applied to van der Waals' state equations. This implies that descending/ascending paths in a hysteretic loop differ thermodynamically, and a criterion underlying this phenomenon may be looked for.

3.2. Cluster Expansion and Virial Coefficients

To work out Eq. (5), consider the differential:

$$dP = \left(\frac{\partial p}{\partial T}\right)_V dT + \left(\frac{\partial p}{\partial V}\right)_T dV \tag{6}$$

and the state equation [40]:

$$\beta p\,(V,T) = \rho\,(1 + \Xi) \tag{7}$$

where $\beta = 1/(k_B T)$ (k_B = Boltzmann's constant), $\rho = N/V$ is the nanoparticle number density, evaluated in the cluster volume, and:

$$\Xi(\rho, T; u) = -\sum_{n=1}^{\infty} \frac{n\gamma_n}{1+n}\rho^n \tag{8}$$

is the pressure correction that follows from the concentration activity coefficients in nanoparticle clusters of increasingly higher densities. The term $\gamma_n = \gamma_n(T, u)$ is a functional of the interparticle potential, $u = u(\mathbf{r})$, and is indexed by the $(n+1)$-particle collisions it accounts for, pointing out a succession of virial coefficients at increasing order. To go ahead note that unlike Eq. (6), which is an exact differential, the integrand in Eq. (5) may be not, thus one needs to carry out the cyclic integration explicitly. This may be done by parameterizing the integral with T, and canceling every contribution that is zero upon any (integer) number of loops. Some differential algebra in the end returns:

$$-\oint VdP = \oint \Sigma\, dT \geqslant 0 \tag{9}$$

where Σ stands for a measure of entropy in the solution given by:

$$\Sigma\,(\rho, T, u) = Nk_B(\ln\rho + T\alpha_V\Xi) \tag{10}$$

and α_V is the thermal expansion coefficient. We can see that, in the (T, Σ) plane, the condition equivalent to Eq. (5) is:

$$\Sigma_{i\to f} \leqslant \Sigma_{f\to i} \tag{11}$$

with the aggregation path getting ascending and staying below the dispersion's.

The last two relations denote the statistical thermodynamics result for the occurrence of a hysteresis cycle, which can be useful to inquiry the effects of interparticle forces and get a criterion for the onset of an incipient cycle. Generally, it will depend on the rate at which Ξ converges (i.e. on the nanoparticle cluster density) as, for any system, there will be a minimum order to take into account for this condition to hold ($n \leqslant \overline{n}$). In our case, disperse systems are definitely dilute (volume fraction $\varphi \approx 1.7 \cdot 10^{-5}$) and inspecting the second virial coefficient of the nanoparticle phase in the liquid should suffice to catch at least the main physical traits of our experiments. It is also worthwhile to remind that the successful employment of second virial coefficients in colloid and interface science has a long history (see e.g. [41]), going from adhesive hard-sphere fluids [42] to more complex mean-force interaction potentials, as protein-protein and protein-salt [43,44], where applicability of virial corrections and (modified) DLVO theories still hold [45,46].

3.3. Virtual Work Principle for Incipient Hysteresis

3.3.1. Isothermal Variation

We specialize Eq. (11) to central pairwise forces with second virial coefficient [40]:

$$B_2 \equiv -\frac{1}{2}\gamma_1 = -\frac{1}{2}\int \mathrm{f}(r)\, d^3r \tag{12}$$

and Mayer's function $\mathrm{f}(r) = \mathrm{e}^{-\beta u(r)} - 1$. For an isothermal transform, Eq. (11) is translated into:

$$\frac{1}{\langle\alpha_V\rangle T}\ln\left(\frac{\rho_{f\to i}}{\rho_{i\to f}}\right) \geqslant (\rho B_2)_{i\to f} - (\rho B_2)_{f\to i} \tag{13}$$

where $\langle\alpha_V\rangle$ is the mean thermal expansion coefficient of a cluster over a loop. Eq. (13) is linking, for any temperature value of ascending/descending paths, the cluster density to nanoparticle forces and it is well posed, as the inequality changes sign consistently upon reverting the path order. The second virial coefficient now can be well approximated to the sum of a constant covolume (V_c) and one more interaction term outside the nanoparticle hard core space [40]:

$$B_2(u) = \frac{\beta}{2}\int u(\mathbf{r}) d^3r + V_c \tag{14}$$

We are seeking a criterion which is as general as possible, independent of the hysteresis region it is applied to. Thence, as long as [47] $T\langle\alpha_V\rangle \sim 10^{-2} - 10^{-1}$ and dilution is so high, volume fraction corrections brought by V_c may be neglected in the first place. Eq. (13) now can be perturbed by a small hysteresis cycle, pointing out a sort of virtual work principle [48] for clustering at the onset of hysteresis formation, and it is interesting to note the conceptual matching between our theoretical approach (Fig. 4) and and the transient equilibrium mapping described in the experimental section (Fig. 2a). Let $\overline{V}$ be the volume of an unperturbed cluster, we need to perturb both sides in Eq. (13) by a small volume (that is, $\delta v \ll \overline{V}$). By retaining terms at first order, calculations performed in Supporting Information B yield a couple of conditions.

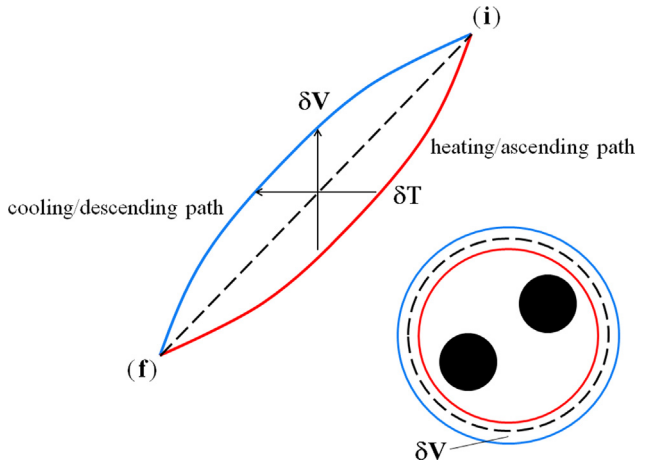

Fig. 4. Variational scheme at the hysteretic onset for a 2-nanoparticle cluster, with the used notations for both isothermal and isochoric patterns.

The first is a mean energy bound at the unperturbed state that may be finally expressed as:

$$\langle u\rangle_{\overline{S}} = \langle u_{\overline{V}}\rangle + \langle E_0\rangle \tag{15}$$

where $\langle u\rangle_{\overline{S}}$ is a mean surface potential, $\langle E_0\rangle = 2k_B/(N\langle\alpha_V\rangle)$ and $\langle \dots {}_V\rangle$ is a volume averaging, generally defined over a domain $\mathbf{\Gamma}$ as:

$$\langle \mathrm{g}_{\Gamma}\rangle \doteq \frac{1}{\Gamma}\int_{\Gamma} \mathrm{g}\, d^3r \qquad (\Gamma > V_c) \tag{16}$$

for any test function g that is continuous in space (outside V_c). Thermal fluctuations get negligible in thermodynamic limit ($N\to\infty, \overline{V}\to\infty, \overline{\rho}$ = const.), reducing Eq. (15) to an identity relation for surface and volume averages. Otherwise, an effective temperature scale appears in Boltzmann's $\langle E_0\rangle$ via the thermal expansion coefficient and, for a representative cluster of $N\approx 5-10^2$ units [49] taking the former range of $\langle\alpha_V\rangle$ values, one obtains $\langle E_0\rangle = \nu k_B T$ with $\nu\sim 0.1-20$. This energy excess identifies the activation barrier for cluster formation in unperturbed states. In Fig. 5, aggregation and dispersion states are disposed to respect the nanoclustering trends along a hysteresis loop, heating cycles being linked overall to a larger aggregation extent, and intervals on the abscissa generally represent distances in thermodynamic plane. The second condition is variational and regards an incipient cycle. Let $\mathrm{u}_i \equiv u_{i\to f} - u_{f\to i}$, calculations return:

$$\langle \mathrm{D}_{\nu}\mathrm{u}_i\rangle < 0 \tag{17}$$

where, for notational simplicity, $\mathrm{D}_x \equiv \delta/\delta x$ and subindex $\overline{V}$ is omitted from volume averages. Eq. (17) is to be basically conducted upon parameter changes (e.g. in the interparticle potential) of two close hysteretic paths and, along with Eq. (15), determines a minimal criterion to expect hysteresis in isothermal clustering of colloid nanoparticles. Consistently, the condition $\mathrm{u}_i\to 0^+$ is representative of particle clusters in unperturbed states. The applied work perturbations are meant in fact to be 'virtual' (time being not explicitly introduced). To illustrate the criterion, Fig. (6) reports a qualitative diagram that is reminiscent of Eyring's model for momentum transport [50]. In that view, the energy profile decreases in the motion direction while here it is predicted to lower on going from heating to cooling paths, i.e. in the directions of virtual work ($\delta V>0$), heat flux ($\delta T<0$) and pressure drop ($\delta p<0$) (Fig. 6). When a cooling/heating rate is introduced, the activation barrier at the unperturbed state gets distorted by the perturbation in Eq. (17).

To close this subsection, we believe that the prerequisites beneath Eqs. (15, 17) should be inquired as well in the dynamical picture underlying possible clustering oscillations, i.e. a multiplicity of separate energy states laying between descending and ascending paths. Other authors had formerly come to an alike conclusion, although on a different ground (e.g. nonlinearity) and in chemically reacting systems, whose formal description differs from colloid assembly to some extent [51].

3.3.2. Isochoric and Isothermal Variations

To describe the onset of a most general hysteretic loop, the variation from isochoric patterns should be also regarded in Σ. As interparticle potentials in colloids are temperature dependent, such a contribution basically stems from varying $T\Xi$ between states $T\pm\delta\mathrm{t}$ ($i\rightleftharpoons f$) with $\delta\mathrm{v}=0$. Expanding the function u in the neighbourhood of T and operating as in the former subsection imply that:

$$\mathrm{D}_{\mathrm{t}}(\alpha_V T\rho B_2) = \langle \mathrm{D}_{\mathrm{t}}\mathrm{u}_i\rangle - \left\langle\frac{\partial \mathrm{U}_i}{\partial T}\right\rangle - 2k_B\frac{V_c}{\overline{V}} \tag{18}$$

is the energy functional derivative to be accounted for in Eq. (13), with $\mathrm{U}_i \equiv u_{i\to f} + u_{f\to i}$. On this basis, Eq. (15) and Eq. (17) for an arbitrary cluster of volume V and surface S get refined respectively by:

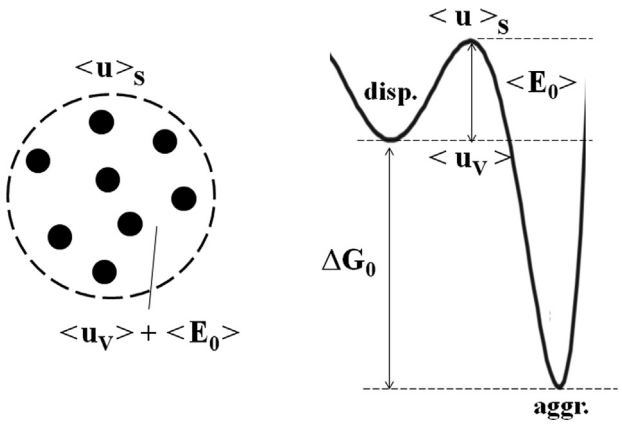

Fig. 5. Scheme of energy/thermodynamic states in a clustering system near/at unperturbed states. Eq. (15) is illustrated for a nanoparticle cluster ($N=8$, left side). On the right activation and Gibbs free energies are depicted, being $|\Delta G_0| = |\Delta H_0 - T\Delta S_0| \approx 20\, k_B T$ ($T\approx T_r$) and $\langle E_0\rangle \sim (0.1-20)\, k_B T$ ($N\sim 5-10^2$). Relative disposition of dispersion and aggregation states was chosen according to the positions of cooling and heating cycles in the thermodynamic plane. Diagram is not on scale.

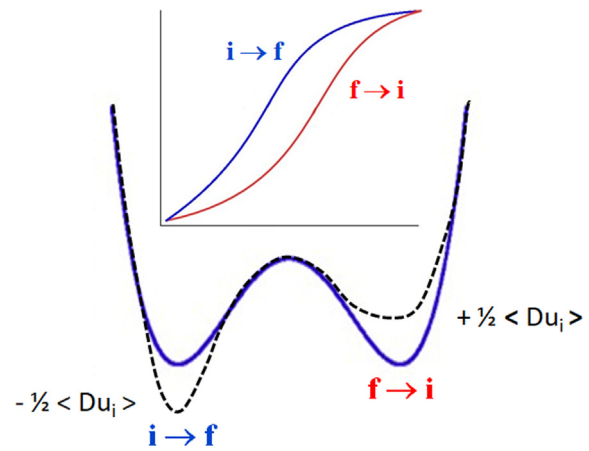

Fig. 6. Eyring-like scheme, where the unperturbed profile (blue magenta) depicts for simplicity an energy excess barrier ($\sim\langle E_0\rangle$) between two states at equal dispersion degree. $\langle \mathrm{Du}_i\rangle$ may both follow from temperature and volume variations in Eq. (20). Diagram is not on scale.

$$\left\langle u\right\rangle_S \;=\; \langle u_V\rangle \;+\; \frac{1}{\langle\alpha_V\rangle}\frac{\partial\langle u_V\rangle}{\partial T} \;+\; \langle E\rangle \tag{19}$$

$$\langle \mathrm{D_v u_i}\rangle \;+\; \frac{1}{\langle\alpha_V\rangle V}\,\langle \mathrm{D_t u_i}\rangle \;<\; 0 \tag{20}$$

where, for a dilute solution, it is still:

$$\langle E\rangle \;\approx\; \langle E_0\rangle \tag{21}$$

with $\langle E_0\rangle$ still keeping the meaning of a thermal barrier (see the conclusive part of Supporting Information B).

4. Theoretical Results and Discussion

Hysteretic nanoclustering in solution is explained here by means of entropy and enthalpy functions interplaying via the interparticle potential. As confirmed by the present and other observational studies [31,35], both isothermal and thermal hysteresis turn out to be feasible phenomenologies, the high temperature sensitivity displayed by colloid forces (especially of repulsive terms) being crucial to trigger the thermal response. We observe that this picture would come to support as well a dual hysteretic behavior of T in the variable V, which is likely harder to be detected.

We now go ahead with examining the two deduced relations, Eq. (19) and Eq. (20), in light of the available experimental and theoretical information. The latter is the most important, as it introduces an asymmetry component for the hysteretic pressure. Interestingly, this also conforms to a latest work on the slow assembly/disassembly kinetics in supramolecular reactions, the sharp line dividing the two processes in (T,ρ) plane being conceived as an uncountable set of equilibrium positions (i.e. the locus point upon $\delta\mathrm{v}\to 0^+$) [37]. A 'transient equilibrium mapping' model was thereby derived to justify hysteresis of cooling/heating paths and to determine thermodynamic data of slowly (non-covalent) monomer dis/assembling. This hypothesis was tested by numerical simulations and, for any T value, the trend of free monomer fractions detected therein is in line with the pressure drop foreseen by Eq. (20) across a minimal loop. Furthermore, we were able to consistently reproduce the results of this mapping analysis within our experimental context as well.

4.1. Energy Bound

First note that either the thermodynamic or infinite dilution limit of a purely isochoric transform would lead to $\langle u\rangle_S, \langle u\rangle_V$ and $\langle E_0\rangle\to 0$ (Eq. 15), therefore to a potential function independent of T, which is not the case of colloid particles. Variations of the isothermal type thus are expected to always contribute to hysteresis. Secondly, as it was already pointed out, $\langle u\rangle_S$ arises as a matter of modelling and mathematical necessity for defining a cluster. The real observable in Eq. (15) is $\langle u_V\rangle$, as it may be experimentally linked to pairwise potentials (or correlation functions). In order to evaluate it, we may adopt the usual DLVO sum $u=u_r+u_a$ of repulsive electrostatic (u_r) and attractive van der Waals (u_a) energy functions, in a form that better suits applications to spherical particles at the nanoscale [52]:

$$u_r(\rho) \;=\; \pi\epsilon\sigma\psi^2\ln\{1+\exp[-\sigma\kappa(\rho-1)]\} \tag{22}$$

$$u_a(\rho) \;=\; -\frac{1}{12}\,A_h\Big[\rho^{-2}+\left(\rho^2-1\right)^{-1}+2\ln\left(1-\rho^{-2}\right)\Big] \tag{23}$$

in which $\rho=r/\sigma>1$ denotes the radial distance between neighbouring particle centers in unit of hard-sphere diameter $\sigma=(3V_c/2\pi)^{1/3}$, ψ is the nanoparticle surface potential, $1/\kappa$ is Debye's length, A_h is Hamaker's constant and ϵ is the absolute static permittivity of the solvent. Since short-range repulsions were regarded by the hard-core's, other terms won't be accounted for. This is also consistent to a distance of closest approach reaching $\rho\approx 1$, as it was determined in experiments on high aggregation states.

Volume average of the total pairwise potential turns out to be negative definite inside a cluster and increasing to zero with increasing radius (R_c). Supporting Information C reports a quantitative analysis in terms of colloid properties, aimed at an estimation of the cluster size at the unperturbed state from the decay length of $\langle u_V\rangle$, here defining a sort of extended $1/\kappa$ for a large enough cluster. Best fits $|\langle u_V\rangle|\sim\exp(-\rho_c/\xi)$ were first conducted in $\rho_c=\kappa R_c$ to obtain a phenomenological correlation length per cluster (ξ), from which at a fixed T a mean radius in physical units follows ($\overline{R}_c\sim\xi/\kappa$). For given values of the initial salt (NaCl) concentration, $c_\pm=0.08, 0.1, 0.2$ M, we get respectively $(150-540)$, $(100-340)$, $(80-280)$, i.e. orders of magnitude that are in accord with the experiments [35] and DLVO studies [53,49], reporting $\overline{R}_c$ to lower with increasing attraction. Best-fitted ranges were stable, as they were mostly influenced by $c_\pm$ via Debye's length, i.e. $\kappa^2=2q_e^2\beta I_\pm/\epsilon\approx 10.82\,c_\pm$ [nm^{-2}], $I_\pm\equiv c_\pm$ being the ionic strength for a $1:1$ electrolyte and q_e denoting the electron charge [41]. Hamaker's constant was set to $A_h\sim 2.5\cdot 10^{-19}$ J [54]. he volume of nanoclusters which stems from the characteristic decay length of their bulk energy here may translate the concept of accessible volume found in other models [33]. It should however be remembered that their values hereby calculated descend from a volume average and are not supposed to have a dynamic significance.

We then tested the influence of a finite collision length added to the integration domain ($\rho>1+2s/\sigma$, with $s\sim 0.5$ nm) [52] to mimic the steric effect from the thickness of ligand layer molecules (BSPP), but in our dilution regime it negligibly affected the extrapolated $\overline{R}_c$ values. This, evidently, does not mean BSPP molecules are unimportant, as they prevent particles from irreversibly accommodating in the deep primary minima of pairwise potentials, an eventuality which would impair the present approach. Note then that surfactant molecules were not used here. However, CTAB layer contribution to Hamaker's forces is known [54] as well to establish at very short separation distances (<1 nm). By dealing in fact with a 3-fold medium, with each layered domain (CTAB-H_2O-CTAB, Au-CTAB-Au, Au-CTAB-H_2O) being assigned an own Hamaker constant, the structure of the attractive interaction within $\sim\xi$ would be still well approximated by a single A_h (for Au-H_2O-Au, see Supporting Information C).

Supporting Information D discusses the thermal variation of the volume average by working in powers of $1/R\equiv\sigma/R_c$, a geometric control parameter taking here on the order of magnitude $\sim 10^{-1}$ ($\sigma=13.4$ nm). Starting from dominant dependencies in repulsive and attractive contributions as a function of ρ_c, it turns out a series expansion of $\partial\langle u_V\rangle/\partial T$ in R^{-m} ($m\geqslant -1$). By gathering every order up to the second and comparing the temperature derivatives of A_h, ψ^2, κ and ϵ_s (relative permittivity) in Eq. (22) prove to be sufficient to deduce that, for a large enough cluster ($1/R\leqslant 10^{-2}$), the prevailing behavior in our parameter range is Debye's $\partial\kappa/\partial T$, i.e.:

$$\frac{\partial\langle u_V\rangle}{\partial T}\;\propto\;-\epsilon\psi^2R_c\left(\kappa\sigma+\frac{1}{\kappa\sigma}\right)\frac{\partial\ln(T\epsilon_s)}{\partial T}\;>\;0 \tag{24}$$

which is positive because the partial derivative on the right, for a NaCl solution in our measurement conditions, is negative [55]. According to Eq. (24) there will exist a minimum value T_m (and correspondingly a minimum cluster radius) below which hysteresis should not be defined, $\partial\langle u_V\rangle/\partial T\leqslant 0$ ($T\leqslant T_m$). Thermal variations of Hamaker's constant act here at second order, $\partial A_h/\partial T=0$ implies

$\partial\langle u_V\rangle/\partial T > 0 \ \forall R \in [0,\infty]$. Since minimum clusters with $R \approx 1$ are found to assemble at low T, one may conclude that in our experiments A_h can be regarded as it were independent of temperature, an approximation which is often used in colloid science.[41]

4.2. Onset of Hysteretic Variations

While use of ligand molecules (BSPP) down to the scale of contacting nanoparticles preserves reversibility of the aggregation process, we have seen in the present view that thermal modulation of clustering should mostly be ascribed to repulsive interactions. Details on the calculus of variations describing nanoparticles assembling upon the dominance of electrostatic forces are collected in Supporting Information E, at the end of which Eq. (20) turns out to be equivalent to:

$$\left(\frac{\delta c_\pm}{\delta V}\right) > \frac{1}{\langle\alpha_V\rangle V}\,\mathscr{R}(c_\pm, T) \tag{25}$$

with:

$$\mathscr{R}(c_\pm, T) = \frac{h_k\partial \ln \epsilon_s/\partial T + \partial \ln(\psi^2/T)/\partial T}{h_k\partial \ln(\epsilon_s/c_\pm)/\partial c_\pm + \partial \ln(c_\pm\psi^2)/\partial c_\pm} > 0 \tag{26}$$

$$h_k \approx h^* + \frac{1}{2\pi^2}(\kappa\sigma)^2 \qquad (h^* = \text{const.}) \tag{27}$$

Positiveness of Eq. (26) is both supported by the established trend of $\epsilon_s = \epsilon_s(c_\pm, T)$ for a watery NaCl solution [55], and our data for the zeta potential $\zeta = \zeta(c_\pm, T)$. In fact, even though ψ values differ from ζ's (normally [56] $|\psi| > |\zeta|$), the analysis in Supporting Information F in terms of ϵ_s, ζ, z (solid surface distance to the slipping plane) and r_s (hydrodynamic radius) is proving that both the numerator and denominator in Eq. (26) carry a negative sign, at least in our domain. A more crucial point on our ζ data instead is about their fluctuations and sensitivity upon aggregation, preventing us from figuring out to which extent they may exactly refer to single particles or particle clusters. At any rate, from Eq. (25), for the cluster volume change between cooling and heating cycles to be $\delta V > 0$ (as it is found experimentally), an increment $\delta c_\pm > 0$ should take place. Such a prediction is drawn in Fig. (7), either displaying the expected profiles of an effective concentration of bulk free ions ($c_{\pm\text{eff}}$) or ψ. Another hint from Eq. (26) is that an hysteresis measure may be settled to be proportional to $1/\mathscr{R}$, and consistently increases with $\sim \langle\partial V/\partial T\rangle$ i.e. with increasing (the mean) thermal expansivity of nanoparticle clusters.

The molecular origin of hysteresis seems to be reflected into a joint behavior of $\delta c_\pm, \psi, \kappa$, rather than into a single effect. A surface potential whose modulus increases with decreasing T (as it is here) thus gets compatible with higher aggregation states and the establishment of hysteresis. A synoptic sketch of the phenomenology is reported in Fig. (8). Upon cooling, $c_{\pm\text{eff}}$ lowers and $|\psi|$ increases, it is surely unsurprising that (exothermic) adsorption or complexation phenomena may be enhanced by decreasing T. Alongside, the prevailing effect of shrinking $1/\kappa$ (versus T) paves van der Waals forces a way to higher and higher aggregation states. On heating the samples, such mechanisms are reverted, the expansion of $1/\kappa$ driving a gradual cluster redispersion. Here, smaller surface potentials allow for stronger aggregation states than in cooling paths. This discharging condition, $|\psi|_{f\to i}(T) < |\psi|_{i\to f}(T)$, along with a slower ion release, $c_{\pm\text{eff}\,f\to i}(T) < c_{\pm\text{eff}\,i\to f}(T)$ (Eq. 25), is a feature of this hysteresis process.

To better grasp the implications of the present model, further studies at nanoscopic or mesoscopic scales will be necessary. What does seem reasonable to state for now is that cooling and heating paths may promote the redistribution of energy states, as it similarly takes place in other thermal processes (e.g. annealing). Clusters may be conceived as similar to heat engines, with a net expansion work per cycle by exchanging heat to their environment. When they pass from releasing to absorbing heat, the amount of work associated with $\Sigma\,\delta T$ (see Eq. 9) is expected to be proportional to the hysteresis area element subtended by δT. As a microscopic interpretation, it may be reasonable to suppose that the molecular order gained in the cooling path transforms into work upon heating, with entropy exchange between nanoclusters and solution. In this view electrochemistry plays a basic role, with Debye's length driving the path evolution and electric double layers being subjected to a (likely) restructuring process. Further nanoparticle contributions, however, were seen to emerge at successive numerical orders. Particularly, it will be interesting to clarify how BSPP molecules may participate in the process envisaged here, as they could interplay not only with Au nanoparticles but also with the electrolyte solution, and affect the solid/liquid interfacial states (by a temperature sensitive surface coverage, to make a meaningful example).

We conclude this section by a couple of remarks on the concept of control parameter for this process. The present nanoclustering phenomenon differs from and is much more complicated than a single particle subjected to some standard thermodynamic cycle, one of the reason lying in a more complex interaction picture establishing in the disperse nanosystem. Along a hysteresis loop,

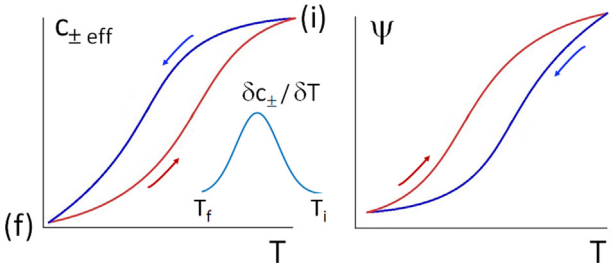

Fig. 7. Prediction for the salt concentration perturbation and surface potential during hysteresis according to Eqs. (25, 26)the general phenomenology in Fig. (8). Note that they compensate each other as their trends are reverted ($\psi < 0$). The quantity $c_{\pm\text{eff}}$ denotes an effective free ion concentration in solution. In the insert on the left is a perturbation example $\delta c_\pm/\delta T$, ideally annulling at the extremes and reaching a maximum at some intermediate temperature. Diagrams are not meant to be on scale, perturbations could be slight.

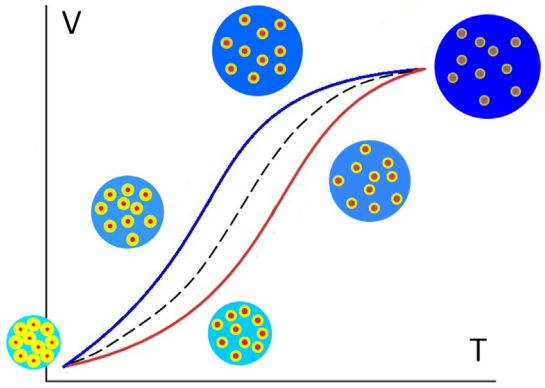

Fig. 8. Pictorial representation of the main electrochemical quantities along a hysteresis loop, where color gradation is proportional to their absolute value: $c_{\pm\text{eff}}$ (blue), κ (yellow), ψ (red). To highlight the dominance of $\kappa = \kappa(T)$, a further thickness effect (yellow) is introduced to depict the electrostatic screening strength. Areas of nanoparticle clusters ($N = 10$) are meant to be proportional to their volume and thus to the dispersion degree. We remark that the above representation illustrates a general mechanism propagating homogeneously along an ideal thermodynamic cycle. It is clearly unintended to furnish a point-by-point description.

nanoparticles experience variations in their potential energies, certainly affecting the effective volume accessible to them. This gives us the possibility of tuning the process by means of a number of control parameters that can be regulated from the outset (e.g. salt molar fraction, dielectric constant, chemical composition of nanoparticles, etc.). In the next section, we will test how two of these control parameters can modulate the hysteresis extent, and thence the net nanoclustering work.

4.3. Influence of Salt Concentration and Nanoparticle Size

We conclude this analysis with an application of Eq. (25). Absorbance measurements are in arbitrary units and their quantitative link to our model is unfortunately very tough. However, a proper inspection of the integrating factor may be shown to give an account of the effect of two independent parameters, the initial salt concentration in solution and the nanoparticle size. For the sake of simplicity, the experimental values of both parameters were extracted from our previous work [35].

The former investigation brought to light that the extent of hysteresis is maximized at a given value $c_\pm \equiv c^* \in (75-85)$ mM (see Fig. 9) [35]. We should thus expect $1/\mathscr{R}$ to display an extremal point in the salt concentration, since:

$$\int \delta \ln V \;=\; \langle \alpha_V \rangle \int \frac{\delta c_\pm}{\mathscr{R}} \tag{28}$$

will be proportional to the hysteretic area, for some profile $\delta c_\pm = \delta c_\pm(T)$ that is shaped as in Fig. (7). To prove this assumption, the derivative $\partial\mathscr{R}/\partial c_\pm$ was numerically carried out by developing each term in Eq. (26). All numerical formulas are recalled in Supporting Information G1 and come from the experimental and theoretical results made available so far. As the exact trend of the surface potential is unknown, extrapolated behaviors based on ζ were adopted in its place. In the end the critical concentration, which obeys:

$$\left(\frac{\partial \mathscr{R}}{\partial c_\pm}\right)_{c^*} = 0, \qquad \left(\frac{\partial^2 \mathscr{R}^{-1}}{\partial c_\pm^2}\right)_{c^*} < 0 \qquad (\mathscr{R}\neq 0) \tag{29}$$

turns out for $\sigma = 13.4$ nm to be $c^* \sim 58$ mM. This prediction, reasonable on the one hand, may suffer however from the approximations made, especially on surface potential. We clearly expect that being able to make a direct use of ψ will yield a better outcome. In fact it sufficed to slightly augment $(\partial \ln \zeta^2/\partial T)$ vs $c_\pm$ in the computation (say, a more responsive force field) to improve the agreement with the experiments (e.g. an enhancement factor $\sim 1.3-1.5$ restores $c^* \in 75-85$ mM).

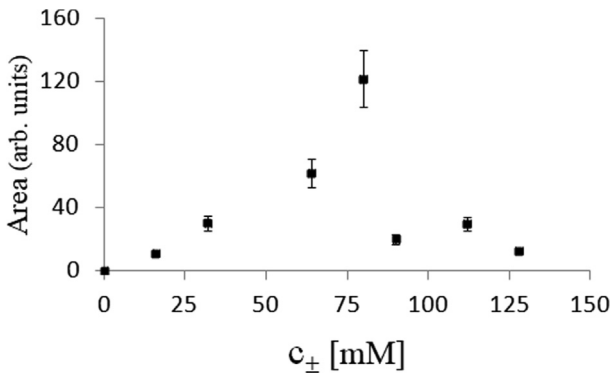

Fig. 9. Hysteresis area versus the initial salt concentration in solution ($T = T_r$). Data derived from Fig. (3b) of previous work.[35].

About the influence of nanoparticle size, the previous work pointed out that the loop area increases with increasing σ. The inquired range was $\sigma = (10-40)$ nm although, for not exceedingly large diameters, it looks reasonable to expect a monotonic trend. Still in line to the former analysis, Eq. (28) has been numerically integrated in $T \in [T_f, T_i]$ to build up the behavior of hysteretic area vs σ (Supporting Information G2). A number of forms were adopted as a profile for $\delta c_\pm$, going from Gaussian functions with variable selectivity (i.e. variance) to cosine's. Reproduction of results only depended upon a perturbation constant and displayed an excellent stability with respect to $\delta c_\pm/\delta T$, supporting the well-posedness of the integrating factor in Eq. (28). This agreement is finally described in Fig. (10), where the hysteresis area is ascertained to scale just as $\propto \sigma^2$.

5. Conclusive Remarks and Future Prospects

A statistical mechanics variational description of thermal hysteresis in reversible clustering of Au nanoparticles has been given as a thermodynamic cycle. This leads to the conceptual scheme in Fig. 11, framing nanoclustering as a heat engine process with potential to produce (useful) work from heat according to the implied state equation and interaction forces at play.

Its behavior can be characterized by a transient equilibrium mapping analysis, here successfully reproduced. The final criterion is elaborated in electrochemistry terms, and mostly depends on a complex interplay of thermal and salt concentration effects, especially via Debye's length κ (e.g. the solvent dielectric constant ϵ_s)

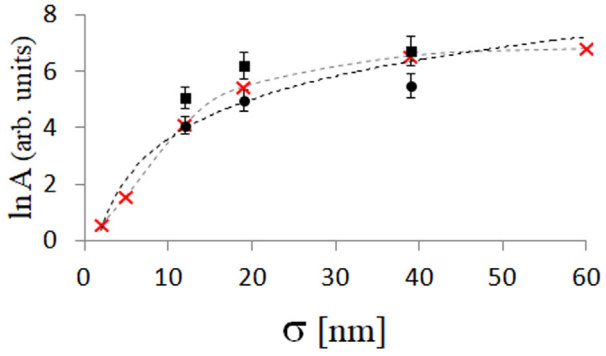

Fig. 10. Behavior of ln(Area) vs σ for two temperature scan rates, 5 K/min. (squares) and 0.2 K/min (circles) (derived from Figs. 5a-b of the former work).[35] Red points indicate the predictions of Eq. (28) for a Gaussian perturbation, $\delta c_\pm/\delta T = \left(a_\varepsilon/\sqrt{2\pi s}\right)\exp-\left[(T-T_r)^2/2s^2\right]$, where a_ε is a perturbation parameter and $s = \frac{1}{8}|T_f - T_i|$ is the root mean square, selecting the hysteresis temperature width around T_r ($T_i \sim 320$ K, $T_f \sim 280K$). In the end, it turns out $a_\varepsilon\langle\alpha_V\rangle = 2.82\cdot 10^{-3}$. Note that the trend originating from the integral model (grey dashed line) is fairly well interpreted by $\ln A \sim 2\ln\sigma - 1$ (black dashed line, R-squared = 0.9712).

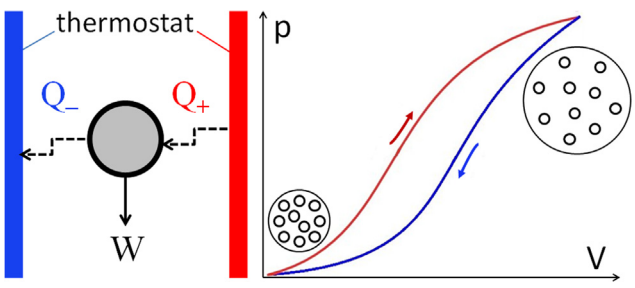

Fig. 11. Illustration of hysteresis in Au nanocolloid clustering as a heat engine process in the (p, V) plane (Q = heat, W = net work).

and surface/zeta potentials (ψ/ζ) of nanoparticles. Our theory well agrees with experimental observations at thermodynamic, nanostructural and electrochemical levels, putting forward a prediction for the hysteretic trend of ψ/ζ (at single particle scales) and for the amount of (free) salt electrolytes in the bulk, here contributing to cycles with higher extents. We finally obtained an integrating factor ($1/\mathscr{R}$) for the cyclic area, which depends on $\kappa\sigma$ and is expressible as the ratio of a differential function of ψ and ϵ_s with respect to $c_\pm$ and T. It was solved numerically to prove that efficiency is maximized for (i) the initial salt concentration taking on a critical value ($c_\pm = c^*$) and (ii) increasing particle diameter ($\sim \sigma^2$). An analogy with Eyring's theory for momentum flux in a fluid is useful to interpret correctly (the virtual) work and heat transports across heating and cooling paths, giving rise to a net pressure drop.

Further efforts now are in order to study the role of interfaces, their electrostatic and elastic features, the adsorption/bound of surface ligands. Also, to determine thermodynamic variables (pressure or volume in addition to temperature) one could study the system at a more local level, detecting nanoclustering fluctuations. At that point, a stochastic Hamiltonian description can be introduced to replace the statistical thermodynamic formalism, but not before having understood the most suitable thermodynamic boundaries of the system and which (free) energy form is to be preserved. Experimentally, description of the system on a single-cluster level is certainly a challenging task, which may benefit by confining nanoclusters within permeable mesoporous shell [57] and tracking the nanoparticle position and velocity in native environment through advanced imaging techniques such as liquid-cell electron microscopy [58].

To close, from a broader perspective, use of plasmonic nanoparticles-based heat engine is a promising approach to extract useful work by means of thermoplasmonic. The remote usage of light energy (and as a work reservoir), one can generate heat locally (within nanocluster volumes) and exploit a fraction of the work for the nanoclustering expansion to elicit e.g. a chemical reaction [59]. Thus, extraction of useful work from nanoparticle-based engine can, in principle, be stored in the form of chemical bonding.

6. Credit Author Statement

S.A.M. - conceptualization, methodology, formal analysis, investigation, visualization, writing - original draft preparation, review & editing; **J.K.** - data curation, validation, investigation; **A. I. I.** - data curation, validation, investigation; **A. A.** - funding acquisition, data curation, validation, resources, writing - editing; **M.G.** - conceptualization, methodology, funding acquisition, resources, supervision, validation, writing - original draft preparation, review & editing;

Declaration of Competing Interest

The authors declare that they have no known competing financial interests or personal relationships that could have appeared to influence the work reported in this paper.

Acknowledgements

A.A. and A.I acknowledge the Grant PID2021-123438NB-I00 funded by MCIN/AEI/10.13039/501100011033 and by "ERDF A way of making Europe", as well as financial support of Eusko Jaurlaritza, code: IT-1566-22 and from the IKUR Strategy. A. I. thanks MICINN for a Personal Técnico de Apoyo contract (PTA2017-14359-I). Correspondence of one of the authors (S.A.M.) with Dezső Boda (IASK/UP - Hungary) is kindly acknowledged. This work was supported by grant PID2019-111772RB-I00 funded by MCIN/AEI/10.13039/501100011033.

Appendix A. Supplementary material

Supplementary data associated with this article can be found, in the online version, at https://doi.org/10.1016/j.jcis.2022.07.037.

References

[1] D. Jiles, D. Atherton, Theory of ferromagnetic hysteresis, J. Magn. Magn. Mater. 61 (1986) 48–60.
[2] O. Boser, Statistical theory of hysteresis in ferroelectric materials, J. Appl. Phys. 62 (1987) 1344–1348.
[3] P.W. Bridgman, The thermodynamics of plastic deformation and generalized entropy, Rev. Mod. Phys. 22 (1950) 56–63.
[4] K.R. McCall, R.A. Guyer, Equation of state and wave propagation in hysteretic nonlinear elastic materials, J. Geophys. Res. Solid Earth 99 (1994) 23887–23897.
[5] H. Janocha, K. Kuhnen, Real-time compensation of hysteresis and creep in piezoelectric actuators, Sens. Actuators A 79 (2000) 83–89.
[6] D.J. Late, B. Liu, H.S.S.R. Matte, V.P. Dravid, C. Rao, Hysteresis in single-layer mos2 field effect transistors, ACS Nano 6 (2012) 5635–5641.
[7] A. Badía, C. López, Vector magnetic hysteresis of hard superconductors, Phys. Rev. B 65 (2002) 104514.
[8] H. Wang, Y. Wu, C. Cong, J. Shang, and T. Yu, Hysteresis of electronic transport in graphene transistors, ACS Nano 4, 7221–7228 (2010a), pMID: 21047068.
[9] E. Kim, C. Kang, H. Baek, K. Hwang, D. Kwak, E. Lee, Y. Kang, E.L. Thomas, Control of optical hysteresis in block copolymer photonic gels: A step towards wet photonic memory films, Adv. Funct. Mater. 20 (2010) 1728–1732.
[10] J. Das, M. Ho, J. Zikherman, C. Govern, M. Yang, A. Weiss, A.K. Chakraborty, J.P. Roose, Digital signaling and hysteresis characterize ras activation in lymphoid cells, Cell 136 (2009) 337–351.
[11] J.E. Ferrell, E.M. Machleder, The biochemical basis of an all-or-none cell fate switch in xenopus oocytes, Science 280 (1998) 895–898.
[12] M. Donohue, G. Aranovich, Adsorption hysteresis in porous solids, J. Colloid Interface Sci. 205 (1998) 121–130.
[13] S.A. Mezzasalma, Hysteresis and isotherm equations in gas-solid adsorption from maximum entropy production, J. Phys. Chem. B 103 (1999) 7542–7550.
[14] A. Giacomello, L. Schimmele, S. Dietrich, Wetting hysteresis induced by nanodefects, Proc. Natl. Acad. Sci. 113 (2016) E262–E271.
[15] W. Choi, A. Tuteja, J.M. Mabry, R.E. Cohen, G.H. McKinley, A modified cassie–baxter relationship to explain contact angle hysteresis and anisotropy on non-wetting textured surfaces, J. Colloid Interface Sci. 339 (2009) 208–216.
[16] M.B. Pinson, T. Zhou, H.M. Jennings, M.Z. Bazant, Inferring pore connectivity from sorption hysteresis in multiscale porous media, J. Colloid Interface Sci. 532 (2018) 118–127.
[17] Effects of hysteresis window on contact angle hysteresis behaviour at large bond number, J. Colloid Interface Sci. 566, 327–337 (2020)
[18] S. Zhu, G. Zhou, W. Yuan, S. Mao, F. Yang, G. Fu, B. Sun, Non-zero-crossing current-voltage hysteresis behavior induced by capacitive effects in bio-memristor, J. Colloid Interface Sci. 560 (2020) 565–571.
[19] M.-P. Valignat, O. Theodoly, J.C. Crocker, W.B. Russel, P.M. Chaikin, Reversible self-assembly and directed assembly of dna-linked micrometer-sized colloids, Proc. Natl. Acad. Sci. 102 (2005) 4225–4229.
[20] G. Maheshwari, G. Brown, D. Lauffenburger, A. Wells, L. Griffith, Cell adhesion and motility depend on nanoscale RGD clustering, J. Cell Sci. 113 (2000) 1677–1686.
[21] J. Baudry, E. Bertrand, N. Lequeux, J. Bibette, Bio-specific recognition and applications: from molecular to colloidal scales, J. Phys. Condens. Matter 16 (2004) R469–R480.
[22] I.D. Mayergoyz, Mathematical models of hysteresis, Phys. Rev. Lett. 56 (1986) 1518–1521.
[23] J. Gan, Z. Mei, X. Chen, Y. Zhou, M.-F. Ge, A modified duhem model for rate-dependent hysteresis behaviors, Micromachines 10 (2019), https://doi.org/10.3390/mi10100680.
[24] T. Geyer, P. Born, T. Kraus, Switching between crystallization and amorphous agglomeration of alkyl thiol-coated gold nanoparticles, Phys. Rev. Lett. 109 (2012) 128302.
[25] Y. Guo, Y. Ma, L. Xu, J. Li, W. Yang, Conformational change induced reversible assembly/disassembly of poly-l-lysine-functionalized gold nanoparticles, J. Phys. Chem. C 111 (2007) 9172–9176.
[26] F. Liu, S. Agarwal, Thermoresponsive gold nanoparticles with positive ucst-type thermoresponsivity, Macromol. Chem. Phys. 216 (2015) 460–465.
[27] X. He, M. Aizenberg, O. Kuksenok, L. Zarzar, A. Shastri, A. Balazs, J. Aizenberg, Synthetic homeostatic materials with chemo-mechano-chemical self-regulation, Nature 487 (2012) 214–218.
[28] S. Semenov, L. Kraft, A. Ainla, M. Zhao, M. Baghbanzadeh, V. Campbell, K. Kang, J. Fox, G. Whitesides, Autocatalytic, bistable, oscillatory networks of biologically relevant organic reactions, Nature 537 (2016) 656–660.
[29] M.N. O'Brien, K.A. Brown, C.A. Mirkin, Critical undercooling in dna-mediated nanoparticle crystallization, ACS Nano 10 (2016) 1363–1368.

[30] S.A. Mezzasalma, L. Grassi, M. Grassi, Physical and chemical properties of carbon nanotubes in view of mechanistic neuroscience investigations. some outlook from condensed matter, materials science and physical chemistry, Mater. Sci. Eng. C 131 (2021) 112480.
[31] D. Wang, B. Kowalczyk, I. Lagzi, B.A. Grzybowski, Bistability and hysteresis during aggregation of charged nanoparticles, J. Phys. Chem. Lett. 1 (2010) 1459–1462, https://doi.org/10.1021/jz100406w.
[32] M. Grzelczak, L.M. Liz-Marzán, R. Klajn, Stimuli-responsive self-assembly of nanoparticles, Chem. Soc. Rev. 48 (2019) 1342–1361.
[33] I. Martínez, d. Roldán, L. Dinis, D. Petrov, J.M. Parrondo, R. Rica, Brownian carnot engine, Nature Phys. 12 (2016) 67–70.
[34] I.A. Martínez, d. Roldán, L. Dinis, R.A. Rica, Colloidal heat engines: a review, Soft Matter 13 (2017) 22–36.
[35] J. Kruse, S. Merkens, A. Chuvilin, M. Grzelczak, Kinetic and thermodynamic hysteresis in clustering of gold nanoparticles: Implications for nanotransducers and information storage in dynamic systems, ACS Appl. Nano Mater. 3 (2020) 9520–9527.
[36] Y.-C. Lin, C.-Y. Chen, H.-L. Chen, T. Hashimoto, S.-A. Chen, Y.-C. Li, Hierarchical self-assembly of nanoparticles in polymer matrix and the nature of the interparticle interaction, J. Chem. Phys. 142 (2015) 214905.
[37] C. Hennecker, C. Lachance-Brais, H. Sleiman, A. Mittermaier, Transient equilibrium mapping: A new tool for measuring the thermodynamics of slowly assembling supramolecular systems, ChemRxiv (2021). 10.33774/chemrxiv-2021-mvjqq.
[38] M.E. Cates, V.N. Manoharan, Celebrating soft matter's 10th anniversary: Testing the foundations of classical entropy: colloid experiments, Soft Matter 11 (2015) 6538–6546.
[39] A. Jódar-Reyes, A. Martín-Rodríguez, J. Ortega-Vinuesa, An enthalpic analysis on the aggregation of colloidal particles studied by microcalorimetry, J. Colloid Interface Sci. 237 (2001) 6–10.
[40] D. Goodstein, States of Matter, Dover Publications Inc, New York, 1985.
[41] J. Israelachvili, Intermolecular and Surface Forces, 3rd ed., Academic Press, San Diego, 2015.
[42] B. Barboy, On a representation of the equation of state of fluids in terms of the adhesive hard-spheres model, J. Chem. Phys. 61 (1974) 3194–3196.
[43] R. Curtis, L. Lue, A molecular approach to bioseparations: Protein–protein and protein–salt interactions, Chem. Eng. Sci. 61 (2006) 907–923.
[44] W. Liu, D. Bratko, J.M. Prausnitz, H.W. Blanch, Effect of alcohols on aqueous lysozyme–lysozyme interactions from static light-scattering measurements, Biophys. Chem. 107 (2004) 289–298.
[45] S. Pusara, P. Yamin, W. Wenzel, M. Krstic, M. Kozlowska, A coarse-grained xdlvo model for colloidal protein–protein interactions, Phys. Chem. Chem. Phys. 23 (2021) 12780–12794.
[46] A.E. Saunders, B.A. Korgel, Second virial coefficient measurements of dilute gold nanocrystal dispersions using small-angle x-ray scattering, J. Phys. Chem. B 108 (2004) 16732–16738.
[47] J. Troncoso, P. Navia, L. Romaní, D. Bessieres, T. Lafitte, On the isobaric thermal expansivity of liquids, J. Chem. Phys. 134 (2011) 094502.
[48] C.L. Dym, Solid Mechanics: A Variational Approach, Advanced Engineering Series, McGraw-Hill, New York, 1973.
[49] E. Mani, W. Lechner, W.K. Kegel, P.G. Bolhuis, Equilibrium and non-equilibrium cluster phases in colloids with competing interactions, Soft Matter 10 (2014) 4479–4486.
[50] R. Bird, W. Stewart, E. Lightfoot, Transport Phenomena, second Edition., John Wiley & Sons, New York, US, 2002. Chap. 23,24..
[51] C.L. Creel, J. Ross, Multiple stationary states and hysteresis in a chemical reaction, J. Chem. Phys. 65 (1976) 3779–3789.
[52] Y. Liu, X. Han, L. He, Y. Yin, Thermoresponsive assembly of charged gold nanoparticles and their reversible tuning of plasmon coupling, Angew. Chem. Int. Ed. 51 (2012) 6373–6377.
[53] T.H. Zhang, J. Klok, R. Hans Tromp, J. Groenewold, W.K. Kegel, Non-equilibrium cluster states in colloids with competing interactions, Soft Matter 8 (2012) 667–672.
[54] S. Biggs, P. Mulvaney, Measurement of the forces between gold surfaces in water by atomic force microscopy, J. Chem. Phys. 100 (1994) 8501–8505.
[55] M. Valiskó, D. Boda, The effect of concentration- and temperature-dependent dielectric constant on the activity coefficient of nacl electrolyte solutions, J. Chem. Phys. 140 (2014) 234508.
[56] R. Hunter, Zeta Potential in Colloid Science, Principles and Applications (Academic Press, London-New York, 386 pages, 1981).
[57] A. Sánchez-Iglesias, N. Claes, D.M. Solís, J.M. Taboada, S. Bals, L.M. Liz-Marzán, M. Grzelczak, Reversible clustering of gold nanoparticles under confinement, Angew. Chem. Int. Ed. 57 (2018) 3183–3186.
[58] A.S. Powers, H.-G. Liao, S.N. Raja, N.D. Bronstein, A.P. Alivisatos, H. Zheng, Tracking Nanoparticle Diffusion and Interaction during Self-Assembly in a Liquid Cell, Nano Lett. 17 (2017) 15–20.
[59] G. Baffou, F. Cichos, R. Quidant, Applications and challenges of thermoplasmonics, Nat. Mater. 19 (2020).